

Measurement of Branching Fractions and Charge Asymmetries in B Meson Decays to $\eta^{(\prime)}K^*$, $\eta^{(\prime)}\rho$, and $\eta'\pi$

The BABAR Collaboration

November 21, 2018

Abstract

We present preliminary measurements of branching fractions and charge asymmetries for the B meson decays $B \rightarrow \eta^{(\prime)}K^*$, $B \rightarrow \eta^{(\prime)}\rho$, and $B^+ \rightarrow \eta'\pi^+$. The data were recorded with the BABAR detector at PEP-II and correspond to 89×10^6 $B\bar{B}$ pairs produced in e^+e^- annihilation through the $\Upsilon(4S)$ resonance. We find the branching fractions $\mathcal{B}(B^0 \rightarrow \eta K^{*0}) = (19.0_{-2.1}^{+2.2} \pm 1.3) \times 10^{-6}$, $\mathcal{B}(B^+ \rightarrow \eta K^{*+}) = (25.7_{-3.6}^{+3.8} \pm 1.8) \times 10^{-6}$, $\mathcal{B}(B^+ \rightarrow \eta\rho^+) = (10.5_{-2.8}^{+3.1} \pm 1.3) \times 10^{-6}$, $\mathcal{B}(B^+ \rightarrow \eta'\rho^+) = (14.0_{-4.6}^{+5.1} \pm 1.9) \times 10^{-6}$ ($< 22 \times 10^{-6}$ with 90% confidence), and $\mathcal{B}(B^+ \rightarrow \eta'\pi^+) = (2.8_{-1.0}^{+1.3} \pm 0.3) \times 10^{-6}$ ($< 4.5 \times 10^{-6}$). We also set 90% CL upper limits of $\mathcal{B}(B^0 \rightarrow \eta'K^{*0}) < 6.4 \times 10^{-6}$ and $\mathcal{B}(B^+ \rightarrow \eta'K^{*+}) < 12 \times 10^{-6}$. The time-integrated charge asymmetries are $\mathcal{A}_{ch}(\eta K^{*0}) = +0.03 \pm 0.11 \pm 0.02$, $\mathcal{A}_{ch}(\eta K^{*+}) = +0.15 \pm 0.14 \pm 0.02$, and $\mathcal{A}_{ch}(\eta\rho^+) = +0.06 \pm 0.29 \pm 0.02$.

Contributed to the XXIst International Symposium on Lepton and Photon Interactions at High Energies, 8/11 — 8/16/2003, Fermilab, Illinois USA

Stanford Linear Accelerator Center, Stanford University, Stanford, CA 94309

Work supported in part by Department of Energy contract DE-AC03-76SF00515.

The BABAR Collaboration,

B. Aubert, R. Barate, D. Boutigny, J.-M. Gaillard, A. Hicheur, Y. Karyotakis, J. P. Lees, P. Robbe,
V. Tisserand, A. Zghiche

Laboratoire de Physique des Particules, F-74941 Annecy-le-Vieux, France

A. Palano, A. Pompili

Università di Bari, Dipartimento di Fisica and INFN, I-70126 Bari, Italy

J. C. Chen, N. D. Qi, G. Rong, P. Wang, Y. S. Zhu

Institute of High Energy Physics, Beijing 100039, China

G. Eigen, I. Ofte, B. Stugu

University of Bergen, Inst. of Physics, N-5007 Bergen, Norway

G. S. Abrams, A. W. Borgland, A. B. Breon, D. N. Brown, J. Button-Shafer, R. N. Cahn, E. Charles,
C. T. Day, M. S. Gill, A. V. Gritsan, Y. Groysman, R. G. Jacobsen, R. W. Kadel, J. Kadyk, L. T. Kerth,
Yu. G. Kolomensky, J. F. Kral, G. Kukartsev, C. LeClerc, M. E. Levi, G. Lynch, L. M. Mir, P. J. Oddone,
T. J. Orimoto, M. Pripstein, N. A. Roe, A. Romosan, M. T. Ronan, V. G. Shelkov, A. V. Telnov,
W. A. Wenzel

Lawrence Berkeley National Laboratory and University of California, Berkeley, CA 94720, USA

K. Ford, T. J. Harrison, C. M. Hawkes, D. J. Knowles, S. E. Morgan, R. C. Penny, A. T. Watson,
N. K. Watson

University of Birmingham, Birmingham, B15 2TT, United Kingdom

T. Held, K. Goetzen, H. Koch, B. Lewandowski, M. Pelizaeus, K. Peters, H. Schmuecker, M. Steinke
Ruhr Universität Bochum, Institut für Experimentalphysik 1, D-44780 Bochum, Germany

N. R. Barlow, J. T. Boyd, N. Chevalier, W. N. Cottingham, M. P. Kelly, T. E. Latham, C. Mackay,
F. F. Wilson

University of Bristol, Bristol BS8 1TL, United Kingdom

K. Abe, T. Cuhadar-Donszelmann, C. Hearty, T. S. Mattison, J. A. McKenna, D. Thiessen

University of British Columbia, Vancouver, BC, Canada V6T 1Z1

P. Kyberd, A. K. McKemey

Brunel University, Uxbridge, Middlesex UB8 3PH, United Kingdom

V. E. Blinov, A. D. Bukin, V. B. Golubev, V. N. Ivanchenko, E. A. Kravchenko, A. P. Onuchin,
S. I. Serebnyakov, Yu. I. Skovpen, E. P. Solodov, A. N. Yushkov

Budker Institute of Nuclear Physics, Novosibirsk 630090, Russia

D. Best, M. Bruinsma, M. Chao, D. Kirkby, A. J. Lankford, M. Mandelkern, R. K. Mommsen, W. Roethel,
D. P. Stoker

University of California at Irvine, Irvine, CA 92697, USA

C. Buchanan, B. L. Hartfiel

University of California at Los Angeles, Los Angeles, CA 90024, USA

B. C. Shen

University of California at Riverside, Riverside, CA 92521, USA

D. del Re, H. K. Hadavand, E. J. Hill, D. B. MacFarlane, H. P. Paar, Sh. Rahatlou, V. Sharma

University of California at San Diego, La Jolla, CA 92093, USA

J. W. Berryhill, C. Campagnari, B. Dahmes, N. Kuznetsova, S. L. Levy, O. Long, A. Lu, M. A. Mazur,
J. D. Richman, W. Verkerke

University of California at Santa Barbara, Santa Barbara, CA 93106, USA

T. W. Beck, J. Beringer, A. M. Eisner, C. A. Heusch, W. S. Lockman, T. Schalk, R. E. Schmitz,
B. A. Schumm, A. Seiden, M. Turri, W. Walkowiak, D. C. Williams, M. G. Wilson

University of California at Santa Cruz, Institute for Particle Physics, Santa Cruz, CA 95064, USA

J. Albert, E. Chen, G. P. Dubois-Felsmann, A. Dvoretzkii, D. G. Hitlin, I. Narsky, F. C. Porter, A. Ryd,
A. Samuel, S. Yang

California Institute of Technology, Pasadena, CA 91125, USA

S. Jayatileke, G. Mancinelli, B. T. Meadows, M. D. Sokoloff

University of Cincinnati, Cincinnati, OH 45221, USA

T. Abe, F. Blanc, P. Bloom, S. Chen, P. J. Clark, I. M. Derrington, W. T. Ford, C. L. Lee, U. Nauenberg,
A. Olivas, P. Rankin, J. Roy, J. G. Smith, K. A. Ulmer, W. C. van Hoek, L. Zhang

University of Colorado, Boulder, CO 80309, USA

J. L. Harton, T. Hu, A. Soffer, W. H. Toki, R. J. Wilson, J. Zhang

Colorado State University, Fort Collins, CO 80523, USA

D. Altenburg, T. Brandt, J. Brose, T. Colberg, M. Dickopp, R. S. Dubitzky, A. Hauke, H. M. Lacker,
E. Maly, R. Müller-Pfefferkorn, R. Nogowski, S. Otto, J. Schubert, K. R. Schubert, R. Schwierz, B. Spaan,
L. Wilden

Technische Universität Dresden, Institut für Kern- und Teilchenphysik, D-01062 Dresden, Germany

D. Bernard, G. R. Bonneaud, F. Brochard, J. Cohen-Tanugi, P. Grenier, Ch. Thiebaux, G. Vasileiadis,
M. Verderi

Ecole Polytechnique, LLR, F-91128 Palaiseau, France

A. Khan, D. Lavin, F. Muheim, S. Playfer, J. E. Swain

University of Edinburgh, Edinburgh EH9 3JZ, United Kingdom

M. Andreotti, V. Azzolini, D. Bettoni, C. Bozzi, R. Calabrese, G. Cibinetto, E. Luppi, M. Negrini,
L. Piemontese, A. Sarti

Università di Ferrara, Dipartimento di Fisica and INFN, I-44100 Ferrara, Italy

E. Treadwell

Florida A&M University, Tallahassee, FL 32307, USA

F. Anulli,¹ R. Baldini-Ferrolì, M. Biasini,¹ A. Calcaterra, R. de Sangro, D. Falciari, G. Finocchiaro,
P. Patteri, I. M. Peruzzi,¹ M. Piccolo, M. Pioppi,¹ A. Zallo

Laboratori Nazionali di Frascati dell'INFN, I-00044 Frascati, Italy

¹Also with Università di Perugia, Perugia, Italy

A. Buzzo, R. Capra, R. Contri, G. Crosetti, M. Lo Vetere, M. Macri, M. R. Monge, S. Passaggio,
C. Patrignani, E. Robutti, A. Santroni, S. Tosi

Università di Genova, Dipartimento di Fisica and INFN, I-16146 Genova, Italy

S. Bailey, M. Morii, E. Won

Harvard University, Cambridge, MA 02138, USA

W. Bhimji, D. A. Bowerman, P. D. Dauncey, U. Egede, I. Eschrich, J. R. Gaillard, G. W. Morton,
J. A. Nash, P. Sanders, G. P. Taylor

Imperial College London, London, SW7 2BW, United Kingdom

G. J. Grenier, S.-J. Lee, U. Mallik

University of Iowa, Iowa City, IA 52242, USA

J. Cochran, H. B. Crawley, J. Lamsa, W. T. Meyer, S. Prell, E. I. Rosenberg, J. Yi

Iowa State University, Ames, IA 50011-3160, USA

M. Davier, G. Grosdidier, A. Höcker, S. Laplace, F. Le Diberder, V. Lepeltier, A. M. Lutz, T. C. Petersen,
S. Plaszczynski, M. H. Schune, L. Tantot, G. Wormser

Laboratoire de l'Accélérateur Linéaire, F-91898 Orsay, France

V. Brigljević, C. H. Cheng, D. J. Lange, D. M. Wright

Lawrence Livermore National Laboratory, Livermore, CA 94550, USA

A. J. Bevan, J. P. Coleman, J. R. Fry, E. Gabathuler, R. Gamet, M. Kay, R. J. Parry, D. J. Payne,
R. J. Sloane, C. Touramanis

University of Liverpool, Liverpool L69 3BX, United Kingdom

J. J. Back, P. F. Harrison, H. W. Shorthouse, P. Strother, P. B. Vidal

Queen Mary, University of London, E1 4NS, United Kingdom

C. L. Brown, G. Cowan, R. L. Flack, H. U. Flaecher, S. George, M. G. Green, A. Kurup, C. E. Marker,
T. R. McMahon, S. Ricciardi, F. Salvatore, G. Vaitsas, M. A. Winter

University of London, Royal Holloway and Bedford New College, Egham, Surrey TW20 0EX, United Kingdom

D. Brown, C. L. Davis

University of Louisville, Louisville, KY 40292, USA

J. Allison, R. J. Barlow, A. C. Forti, P. A. Hart, M. C. Hodgkinson, F. Jackson, G. D. Lafferty, A. J. Lyon,
J. H. Weatherall, J. C. Williams

University of Manchester, Manchester M13 9PL, United Kingdom

A. Farbin, A. Jawahery, D. Kovalskyi, C. K. Lae, V. Lillard, D. A. Roberts

University of Maryland, College Park, MD 20742, USA

G. Blaylock, C. Dallapiccola, K. T. Flood, S. S. Hertzbach, R. Kofler, V. B. Koptchev, T. B. Moore,
S. Saremi, H. Staengle, S. Willocq

University of Massachusetts, Amherst, MA 01003, USA

R. Cowan, G. Sciolla, F. Taylor, R. K. Yamamoto
Massachusetts Institute of Technology, Laboratory for Nuclear Science, Cambridge, MA 02139, USA

D. J. J. Mangeol, P. M. Patel
McGill University, Montréal, QC, Canada H3A 2T8

A. Lazzaro, F. Palombo
Università di Milano, Dipartimento di Fisica and INFN, I-20133 Milano, Italy

J. M. Bauer, L. Cremaldi, V. Eschenburg, R. Godang, R. Kroeger, J. Reidy, D. A. Sanders, D. J. Summers,
H. W. Zhao
University of Mississippi, University, MS 38677, USA

S. Brunet, D. Cote-Ahern, C. Hast, P. Taras
Université de Montréal, Laboratoire René J. A. Lévesque, Montréal, QC, Canada H3C 3J7

H. Nicholson
Mount Holyoke College, South Hadley, MA 01075, USA

C. Cartaro, N. Cavallo,² G. De Nardo, F. Fabozzi,² C. Gatto, L. Lista, P. Paolucci, D. Piccolo, C. Sciacca
Università di Napoli Federico II, Dipartimento di Scienze Fisiche and INFN, I-80126, Napoli, Italy

M. A. Baak, G. Raven
NIKHEF, National Institute for Nuclear Physics and High Energy Physics, NL-1009 DB Amsterdam, The Netherlands

J. M. LoSecco
University of Notre Dame, Notre Dame, IN 46556, USA

T. A. Gabriel
Oak Ridge National Laboratory, Oak Ridge, TN 37831, USA

B. Brau, K. K. Gan, K. Honscheid, D. Hufnagel, H. Kagan, R. Kass, T. Pulliam, Q. K. Wong
Ohio State University, Columbus, OH 43210, USA

J. Brau, R. Frey, C. T. Potter, N. B. Sinev, D. Strom, E. Torrence
University of Oregon, Eugene, OR 97403, USA

F. Colecchia, A. Dorigo, F. Galeazzi, M. Margoni, M. Morandin, M. Posocco, M. Rotondo, F. Simonetto,
R. Stroili, G. Tiozzo, C. Voci
Università di Padova, Dipartimento di Fisica and INFN, I-35131 Padova, Italy

M. Benayoun, H. Briand, J. Chauveau, P. David, Ch. de la Vaissière, L. Del Buono, O. Hamon,
M. J. J. John, Ph. Leruste, J. Ocariz, M. Pivk, L. Roos, J. Stark, S. T'Jampens, G. Therin
Universités Paris VI et VII, Lab de Physique Nucléaire H. E., F-75252 Paris, France

P. F. Manfredi, V. Re
Università di Pavia, Dipartimento di Elettronica and INFN, I-27100 Pavia, Italy

²Also with Università della Basilicata, Potenza, Italy

P. K. Behera, L. Gladney, Q. H. Guo, J. Panetta
University of Pennsylvania, Philadelphia, PA 19104, USA

C. Angelini, G. Batignani, S. Bettarini, M. Bondioli, F. Bucci, G. Calderini, M. Carpinelli, V. Del Gamba,
F. Forti, M. A. Giorgi, A. Lusiani, G. Marchiori, F. Martinez-Vidal,³ M. Morganti, N. Neri, E. Paoloni,
M. Rama, G. Rizzo, F. Sandrelli, J. Walsh
Università di Pisa, Dipartimento di Fisica, Scuola Normale Superiore and INFN, I-56127 Pisa, Italy

M. Haire, D. Judd, K. Paick, D. E. Wagoner
Prairie View A&M University, Prairie View, TX 77446, USA

N. Danielson, P. Elmer, C. Lu, V. Miftakov, J. Olsen, A. J. S. Smith, H. A. Tanaka E. W. Varnes
Princeton University, Princeton, NJ 08544, USA

F. Bellini, G. Cavoto,⁴ R. Faccini,⁵ F. Ferrarotto, F. Ferroni, M. Gaspero, M. A. Mazzoni, S. Morganti,
M. Pierini, G. Piredda, F. Safai Tehrani, C. Voena
Università di Roma La Sapienza, Dipartimento di Fisica and INFN, I-00185 Roma, Italy

S. Christ, G. Wagner, R. Waldi
Universität Rostock, D-18051 Rostock, Germany

T. Adye, N. De Groot, B. Franek, N. I. Geddes, G. P. Gopal, E. O. Olaiya, S. M. Xella
Rutherford Appleton Laboratory, Chilton, Didcot, Oxon, OX11 0QX, United Kingdom

R. Aleksan, S. Emery, A. Gaidot, S. F. Ganzhur, P.-F. Giraud, G. Hamel de Monchenault, W. Kozanecki,
M. Langer, M. Legendre, G. W. London, B. Mayer, G. Schott, G. Vasseur, Ch. Yeche, M. Zito
DSM/Daphnia, CEA/Saclay, F-91191 Gif-sur-Yvette, France

M. V. Purohit, A. W. Weidemann, F. X. Yumiceva
University of South Carolina, Columbia, SC 29208, USA

D. Aston, R. Bartoldus, N. Berger, A. M. Boyarski, O. L. Buchmueller, M. R. Convery, D. P. Coupal,
D. Dong, J. Dorfan, D. Dujmic, W. Dunwoodie, R. C. Field, T. Glanzman, S. J. Gowdy, E. Grauges-Pous,
T. Hadig, V. Halyo, T. Hryn'ova, W. R. Innes, C. P. Jessop, M. H. Kelsey, P. Kim, M. L. Kocian,
U. Langenegger, D. W. G. S. Leith, S. Luitz, V. Luth, H. L. Lynch, H. Marsiske, R. Messner, D. R. Muller,
C. P. O'Grady, V. E. Ozcan, A. Perazzo, M. Perl, S. Petrak, B. N. Ratcliff, S. H. Robertson, A. Roodman,
A. A. Salnikov, R. H. Schindler, J. Schwiening, G. Simi, A. Snyder, A. Soha, J. Stelzer, D. Su,
M. K. Sullivan, J. Va'vra, S. R. Wagner, M. Weaver, A. J. R. Weinstein, W. J. Wisniewski, D. H. Wright,
C. C. Young

Stanford Linear Accelerator Center, Stanford, CA 94309, USA

P. R. Burchat, A. J. Edwards, T. I. Meyer, B. A. Petersen, C. Roat
Stanford University, Stanford, CA 94305-4060, USA

S. Ahmed, M. S. Alam, J. A. Ernst, M. Saleem, F. R. Wappler
State Univ. of New York, Albany, NY 12222, USA

³Also with IFIC, Instituto de Física Corpuscular, CSIC-Universidad de Valencia, Valencia, Spain

⁴Also with Princeton University

⁵Also with University of California at San Diego

W. Bugg, M. Krishnamurthy, S. M. Spanier
University of Tennessee, Knoxville, TN 37996, USA

R. Eckmann, H. Kim, J. L. Ritchie, R. F. Schwitters
University of Texas at Austin, Austin, TX 78712, USA

J. M. Izen, I. Kitayama, X. C. Lou, S. Ye
University of Texas at Dallas, Richardson, TX 75083, USA

F. Bianchi, M. Bona, F. Gallo, D. Gamba
Università di Torino, Dipartimento di Fisica Sperimentale and INFN, I-10125 Torino, Italy

C. Borean, L. Bosisio, G. Della Ricca, S. Dittongo, S. Grancagnolo, L. Lanceri, P. Poropat,⁶ L. Vitale,
G. Vuagnin

Università di Trieste, Dipartimento di Fisica and INFN, I-34127 Trieste, Italy

R. S. Panvini
Vanderbilt University, Nashville, TN 37235, USA

Sw. Banerjee, C. M. Brown, D. Fortin, P. D. Jackson, R. Kowalewski, J. M. Roney
University of Victoria, Victoria, BC, Canada V8W 3P6

H. R. Band, S. Dasu, M. Datta, A. M. Eichenbaum, J. R. Johnson, P. E. Kutter, H. Li, R. Liu,
F. Di Lodovico, A. Mihalyi, A. K. Mohapatra, Y. Pan, R. Prepost, S. J. Sekula, J. H. von
Wimmersperg-Toeller, J. Wu, S. L. Wu, Z. Yu
University of Wisconsin, Madison, WI 53706, USA

H. Neal
Yale University, New Haven, CT 06511, USA

⁶Deceased

1 Introduction

We report the results of searches for B decays to the charmless final states¹ $\eta^{(\prime)}K^*$, $\eta^{(\prime)}\rho$, and $\eta'\pi^+$. For decays that are self tagging with respect to the b or \bar{b} flavor we also measure the direct CP -violating time-integrated charge asymmetry, $\mathcal{A}_{ch} = (\Gamma^- - \Gamma^+)/(\Gamma^- + \Gamma^+)$. For charged B decays $\Gamma^\pm \equiv \Gamma(B^\pm \rightarrow \eta^{(\prime)}h^\pm)$, and for $B^0 \rightarrow \eta K^{*0}$ with $K^{*0} \rightarrow K^+\pi^-$ the sign on Γ matches that of the tertiary kaon.

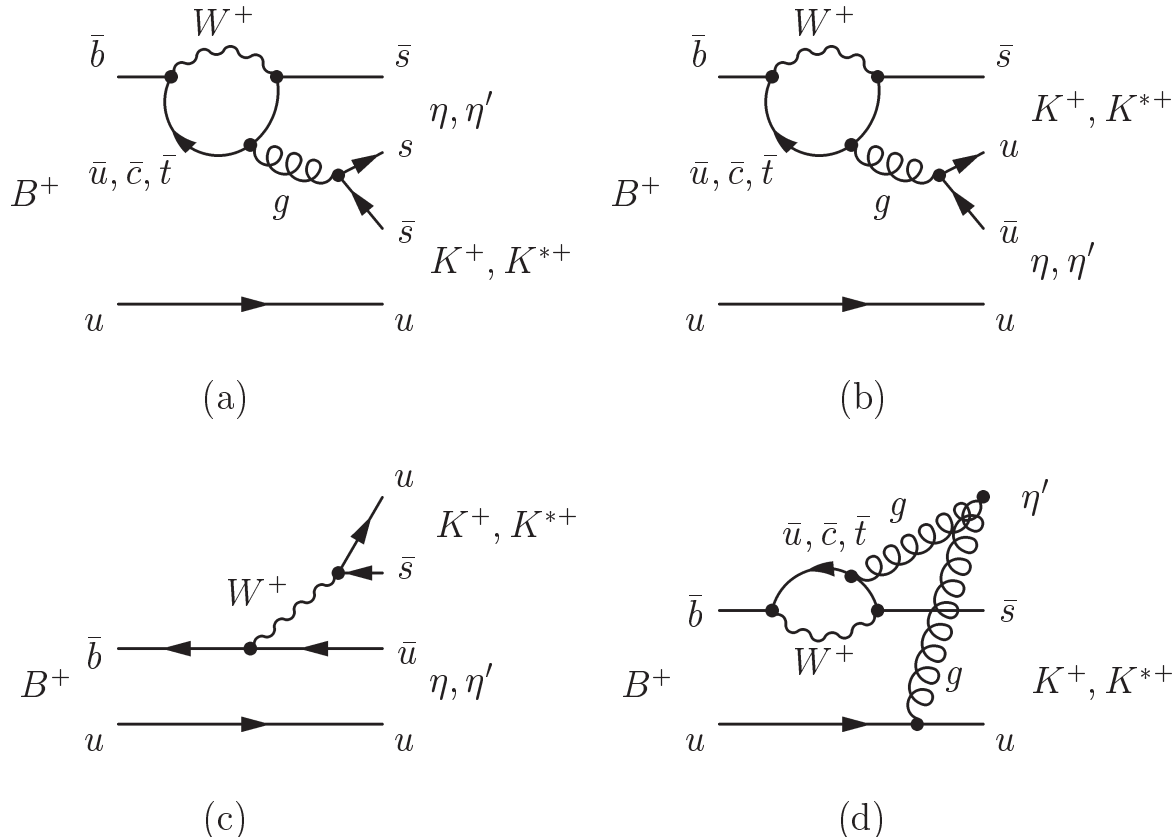


Figure 1: Feynman diagrams for the decays $B \rightarrow (\eta, \eta')(K, K^*)^+$. The neutral decays are similar except that the spectator quark becomes a d , and the tree diagram is internal.

Interest in B decays to η or η' final states intensified in 1997 with the CLEO observation of the decay $B \rightarrow \eta'K$ [1]. It had been pointed out by Lipkin six years earlier [2] that interference between two penguin diagrams (see Fig. 1a and 1b) and the known η/η' mixing angle conspire to greatly enhance $B \rightarrow \eta'K$ and suppress $B \rightarrow \eta K$. Because the vector K^* has the opposite parity from the kaon, the situation is reversed for the $B \rightarrow \eta'K^*$ and $B \rightarrow \eta K^*$ decays. The general features of this picture have already been verified by previous measurements and limits. However the details and possible contributions of flavor-singlet diagrams (*c.f.* Fig. 1d) can only be tested with the measurement of the branching fractions of all four $(\eta, \eta')(K, K^*)$ decays; the branching fraction of the $B \rightarrow \eta'K^*$ decay is expected to be particularly sensitive to a flavor-singlet component [3, 4]. In any case the tree diagrams (Fig. 1c) are CKM suppressed. The results described in this paper

¹Except as noted explicitly, we use a particle name to denote either member of a charge conjugate pair.

complete the measurement of all four decays with a *BABAR* dataset of 89 million $B\bar{B}$ decays [5, 6].

The situation for the decays $\eta^{(\prime)}\rho$ and $\eta'\pi^+$ is different. These decays are expected to be dominated by tree diagrams (see Fig. 2c and 2d) since it is now the penguin diagrams (Fig. 2a and 2b) that are suppressed. Since the internal tree diagram (Fig. 2d) is color suppressed, any interference effect is diluted for these decays. Branching fractions for these decays are generally expected to be in the range $(1-10)\times 10^{-6}$ [7, 8, 9, 10].

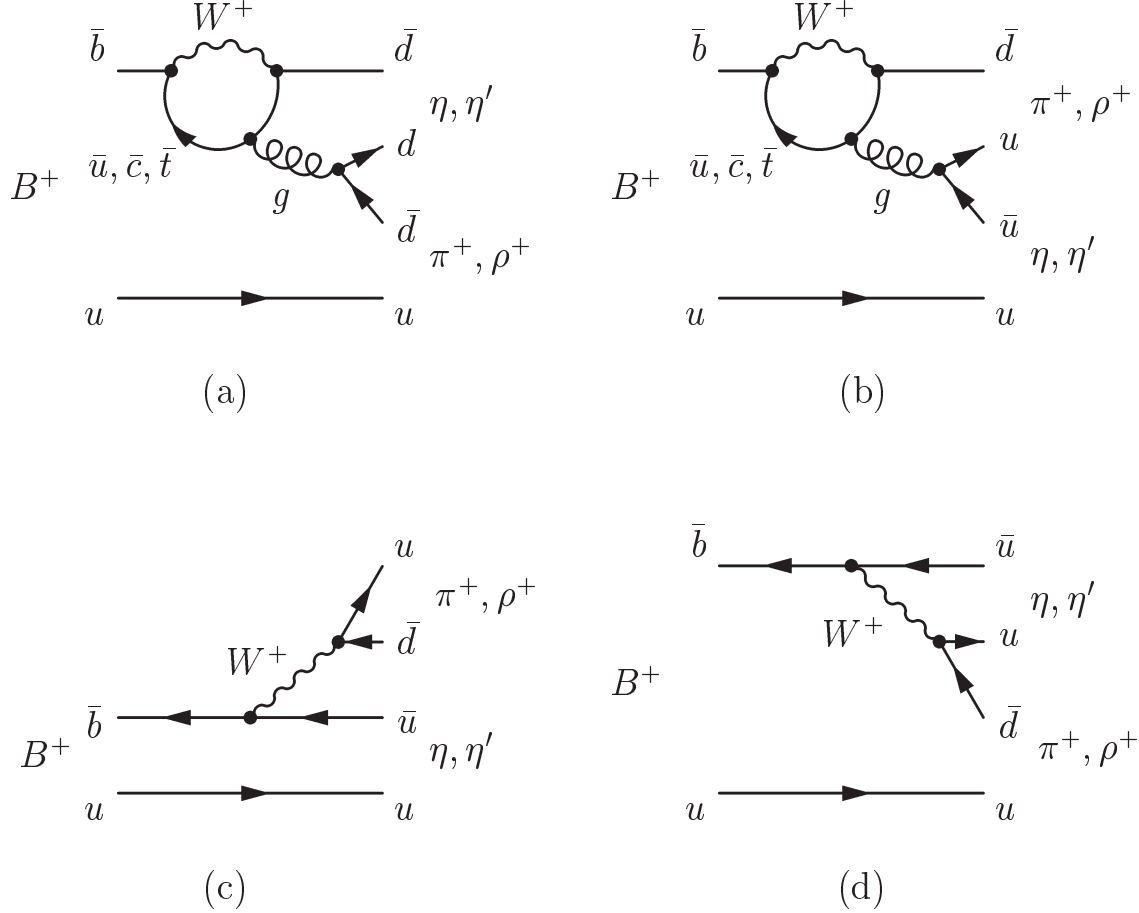


Figure 2: Feynman diagrams for the decays $B^+ \rightarrow \eta\rho^+$, $B^+ \rightarrow \eta'\pi^+$, and $B^+ \rightarrow \eta'\rho^+$.

The charge asymmetry \mathcal{A}_{ch} for most of these decays is expected to be small [7, 11]. However, for the decay $B \rightarrow \eta'\pi$ and $B \rightarrow \eta'K^*$, the penguin and tree diagrams are expected to be of similar magnitude, which allows potentially large charge asymmetries [4, 9, 10, 12].

The current knowledge of these decays comes from published measurements from CLEO [13] and *BABAR* [14], and conference results from *BABAR* [15] and Belle [16]. Tables 1 and 2 summarize these previous results.

2 Detector and Data

The results presented in this paper are based on data collected with the *BABAR* detector [17] at the PEP-II asymmetric e^+e^- collider [18] located at the Stanford Linear Accelerator Center. An

Table 1: Summary of branching fraction results for B decays to η mesons from CLEO [13], previous BABAR [15] measurements, Belle [16], and the present analysis. The results for all fits are given as well as a 90% CL upper limit if given in the cited reference. The overall yields and efficiencies (ϵ) are given as the sum of yields and efficiencies from the daughter particle decay channels. Rows marked (*) refer to measurements that are superseded by the results of the present paper.

Expt.	# $B\bar{B}$ (10^6)	Fit $\mathcal{B}(10^{-6})$	UL $\mathcal{B}(10^{-6})$	Signif. (σ)	Signal yield	ϵ (%)
ηK^{*0}						
CLEO	10	$13.8_{-4.6}^{+5.5} \pm 1.6$	—	5.1	15.6	11.6
BABAR*	23	$19.1_{-5.4}^{+6.3}$	—	5.4	$21.7_{-6.1}^{+7.1}$	4.9
Belle	23	$21.2_{-4.7}^{+5.4} \pm 2.0$	—	5.1	22.1	4.7
This result	89	$19.0_{-2.1}^{+2.2} \pm 1.3$	—	15	157	9.2
ηK^{*+}						
CLEO	10	$26.4_{-8.2}^{+9.6} \pm 3.3$	—	4.8	19.2	7.0
BABAR*	23	$22.1_{-9.2}^{+11.1}$	< 34	3.2	14 ± 7	3.2
Belle	23	—	< 50	2.8	13.8	2.5
This result	89	$25.7_{-3.6}^{+3.8} \pm 1.8$	—	12	113	4.7
$\eta\rho^+$						
CLEO	10	$4.8_{-3.8}^{+5.2}$	< 15	1.3	5.0	11.9
Belle	23	—	< 6.8	0.0	0.0	3.9
This result	89	$10.5_{-2.8}^{+3.1} \pm 1.3$	—	4.8	65	7.0

integrated luminosity of 82 fb^{-1} , corresponding to 89 million $B\bar{B}$ pairs, was recorded at the $\Upsilon(4S)$ resonance (“on-resonance”, center-of-mass energy $\sqrt{s} = 10.58 \text{ GeV}$). An additional 9.6 fb^{-1} were taken about 40 MeV below this energy (“off-resonance”) for the study of continuum backgrounds in which a light or charm quark pair is produced instead of an $\Upsilon(4S)$.

The asymmetric beam configuration in the laboratory frame provides a boost of $\beta\gamma = 0.56$ to the $\Upsilon(4S)$. Charged particles (tracks) are detected and their momenta measured by the combination of a silicon vertex tracker (SVT), consisting of five layers of double-sided detectors, and a 40-layer central drift chamber, both operating in the 1.5-T magnetic field of a solenoid. Photons and electrons (neutral clusters) are detected by a CsI(Tl) electromagnetic calorimeter (EMC).

Charged-particle identification (PID) is provided by the average energy loss (dE/dx) in the tracking devices and by an internally reflecting ring-imaging Cherenkov detector (DIRC) covering the central region.

3 Event Selection

We reconstruct the η mesons in both of the dominant final states $\eta \rightarrow \gamma\gamma$ ($\eta_{\gamma\gamma}$) and $\eta \rightarrow \pi^+\pi^-\pi^0$ ($\eta_{3\pi}$). For the η' , we also reconstruct two final states: $\eta' \rightarrow \rho^0\gamma$ ($\eta'_{\rho\gamma}$) and $\eta' \rightarrow \eta\pi^+\pi^-$ ($\eta'_{\eta\pi\pi}$), with $\eta \rightarrow \gamma\gamma$ (except in the $\eta'_{\eta(3\pi)\pi\pi} K^{*0}$ mode, where we include also $\eta \rightarrow \pi^+\pi^-\pi^0$). The K^{*0} is reconstructed as $K^+\pi^-$ ($K_{K^+\pi^-}^{*0}$), and K^{*+} as either $K^+\pi^0$ ($K_{K^+\pi^0}^{*+}$) or $K_S^0\pi^+$ ($K_{K_S^0\pi^+}^{*+}$), with

Table 2: Summary of branching fraction results for B decays to η' mesons from CLEO [13], previous BABAR [15, 14] measurements, Belle [16], and the present analysis. The results for all fits are given as well as a 90% CL upper limit if given in the cited reference. The overall yields and efficiencies (ϵ) are given as the sum of yields and efficiencies from the daughter particle decay channels. Rows marked (*) refer to measurements that are superseded by the results of the present paper.

Expt.	# $B\bar{B}$ (10^6)	Fit $\mathcal{B}(10^{-6})$	UL $\mathcal{B}(10^{-6})$	Signif. (σ)	Signal yield	ϵ (%)
$\eta'\pi^+$						
CLEO	10	$0.1^{+0.5}_{-0.1}$	< 11.1	0.2	4.4	13.7
BABAR*	23	$5.4^{+3.5}_{-2.6} \pm 0.8$	< 12	2.8	5.7	9.1
This result	89	$2.8^{+1.3}_{-1.0} \pm 0.3$	< 4.5	3.4	13	9.9
$\eta'K^{*0}$						
CLEO	10	$7.8^{+7.7}_{-5.7}$	< 24	1.8	2.4	6.4
BABAR*	54	$4.0^{+3.5}_{-2.4} \pm 1.0$	< 13	1.8	$4.4^{+3.8}_{-2.6}$	1.9
This result	89	$3.2^{+1.8}_{-1.6} \pm 0.9$	< 6.4	2.2	22	6.6
$\eta'K^{*+}$						
CLEO	10	$11.1^{+12.7}_{-8.0}$	< 35	2.5	3.3	3.6
This result	89	$6.1^{+3.9}_{-3.2} \pm 1.2$	< 12	2.4	15	3.0
$\eta'\rho^+$						
CLEO	10	$11.2^{+11.9}_{-7.0}$	< 33	2.4	5.8	5.2
This result	89	$14.0^{+5.1}_{-4.6} \pm 1.9$	< 22	3.8	69	4.1

$K_S^0 \rightarrow \pi^+\pi^-$. The ρ^+ is reconstructed as $\pi^+\pi^0$.

Monte Carlo (MC) simulations [19] of the signal decay modes and of continuum and $B\bar{B}$ backgrounds are used to establish the event selection criteria. The selection is designed to achieve high efficiency and retain sidebands sufficient to characterize the background for subsequent fitting. Photons must have energy exceeding a threshold dependent on the combinatorial background of the specific mode: $E_\gamma > 30$ MeV for the two photons used to reconstruct the π^0 in $\eta \rightarrow \pi^+\pi^-\pi^0$ candidates, $E_\gamma > 100$ MeV for $\eta \rightarrow \gamma\gamma$, and $E_\gamma > 200$ MeV for the photon in $\eta'_{\rho\gamma}$. Additionally, in order to reject background from $B \rightarrow K^*\gamma$ for the ηK^* and $\eta\rho$ analyses, we require that the cosine of the center of mass decay angle for $\eta_{\gamma\gamma}$ daughters, relative to the flight direction of the η , have an absolute value of less than 0.86.

We select resonance candidates with the following requirements on the invariant mass (in MeV) of their final states: $910 < m_{\eta'} < 1000$ for $\eta'_{\rho\gamma}$ and $\eta'_{\eta\pi\pi}$, $520 < m_\eta < 570$ for $\eta_{3\pi}$, $755 < m_{K^*} < 1035$, and $470 < m_{\rho^+} < 1070$. For the $\eta'_{\eta(3\pi)\pi\pi} K^{*0}$ channel, we tighten the K^* mass range to $792 < m_{K^{*0}} < 992$. Since these quantities are observables input to a maximum likelihood fit, the criteria are loose. Additional states are selected with 2-3 sigma cuts: $120 < m_{\pi^0} < 150$, $490 < m_\eta < 600$ for $\eta_{\gamma\gamma}$, tightened to $510 < m_\eta < 580$ in the $\eta'_{\eta\pi\pi}\rho^+$ channel to reduce the amount of continuum background in the sample. For $K_S^0 \rightarrow \pi^+\pi^-$ candidates we require $488 < m_{K_S} < 508$.

In modes with a $K_{K^+\pi^0}^{*+}$ or a ρ^+ , we also require that the cosine \mathcal{H} of the helicity angle (the vector meson's rest decay angle with respect to its flight direction) be greater than -0.5 . For $\eta'_{\eta(3\pi)\pi\pi} K^{*0}$, we require $\mathcal{H} > -0.9$. For K_S^0 candidates we require that the lifetime significance

(τ/σ_τ) be > 3 .

We make several particle identification (PID) requirements to ensure the identity of the signal pions and kaons. Tracks in resonance candidates (excluding the K_S^0) must have DIRC, dE/dx , and EMC responses consistent with the expected particle type. For the $B^+ \rightarrow \eta'\pi^+$ decay, we require that the prompt charged track have an associated DIRC Cherenkov angle between -3.5σ and $+3.5\sigma$ from the expected value for either a pion or a kaon. The Cherenkov angle is used in a subsequent fit to distinguish $\eta'\pi^+$ from $\eta'K^+$.

A B meson candidate is characterized kinematically by the energy-substituted mass $m_{\text{ES}} = \sqrt{(\frac{1}{2}s + \mathbf{p}_0 \cdot \mathbf{p}_B)^2/E_0^2 - \mathbf{p}_B^2}$ and energy difference $\Delta E = E_B^* - \frac{1}{2}\sqrt{s}$, where the subscripts 0 and B refer to the initial $\Upsilon(4S)$ and to the B candidate, respectively, and the asterisk denotes the $\Upsilon(4S)$ frame. The mode-dependent resolutions on these quantities measured for signal events average about 30 MeV for ΔE and 3.0 MeV for m_{ES} . We require $|\Delta E| \leq 0.2$ GeV and $5.2 \leq m_{\text{ES}} \leq 5.29$ GeV.

3.1 Tau, QED, and continuum background

To discriminate against tau-pair and two-photon background we require that each event contain at least three charged tracks, including at least one from the recoil B meson in addition to those required to complete the reconstructed B candidate.

To reject continuum background, we make use of the angle θ_T between the thrust axis of the B candidate and that of the rest of the tracks and neutral clusters in the event, calculated in the $\Upsilon(4s)$ frame. The distribution of $\cos\theta_T$ is sharply peaked near ± 1 for combinations drawn from jet-like $q\bar{q}$ pairs and is nearly uniform for the isotropic B meson decays; we tune the $\cos\theta_T$ cut for each channel to optimize our sensitivity to signal in the presence of continuum background. The resulting requirements are $|\cos\theta_T| < 0.8$ for $\eta_{\gamma\gamma}\rho^+$ and $\eta'_{\eta(3\pi)\pi\pi}K^{*0}$, $|\cos\theta_T| < 0.75$ for $\eta'_{\rho\gamma}K^{*0}$ and $\eta'_{\rho\gamma}K^{*+}$, $|\cos\theta_T| < 0.65$ for $\eta'_{\rho\gamma}\pi^+$ and $\eta'_{\rho\gamma}\rho^+$, and $|\cos\theta_T| < 0.9$ for all of the other decay sequences. The average candidate multiplicity is about 1.1 to 1.2 per event. In events with more than one candidate we accept the one with η or η' mass closest to the nominal value.

The remaining continuum background dominates the samples and is modeled from sideband data for the maximum likelihood fits described in Section 4.

3.2 $B\bar{B}$ background

We use Monte Carlo simulations of $B^0\bar{B}^0$ and B^+B^- pair production and decay to look for possible $B\bar{B}$ backgrounds. Most $B\bar{B}$ backgrounds in these analyses come from a handful of charmless decays with similar final states. To study these backgrounds, we perform our preselection cuts on high statistics MC samples of the prominent $B\bar{B}$ backgrounds. Using our resulting selection efficiency, along with measured (or predicted) branching fractions for the charmless decays in question, we estimate the number of $B\bar{B}$ background events expected to enter our samples from each exclusive charmless decay. From simulated experiments where we embed the expected number of $B\bar{B}$ background events from the MC, we determine whether these backgrounds are large enough to warrant an extra component in the likelihood fit, as described in Section 4.1.

From these studies we find no evidence for significant $B\bar{B}$ backgrounds in either the $\eta \rightarrow \pi^+\pi^-\pi^0$ decay chains or the $\eta'_{\eta\pi\pi}\pi^+$ decay. For the other channels, however, we see evidence for potential $B\bar{B}$ backgrounds, normally involving other charmless B decays with a high-momentum η or η' . Such backgrounds typically are at a level of one or two events and we include a $B\bar{B}$

component in the likelihood fits to discriminate between these backgrounds and the signal. For those channels where we include a $B\bar{B}$ component in the fit, we generate composite $B\bar{B}$ background samples, typically containing events from about five exclusive charmless decay chains.

4 Maximum Likelihood Fit

We use an unbinned, multivariate maximum likelihood fit to extract signal yields for our modes. A sub-sample of events to fit for each decay channel is selected as described in Section 3. The sample sizes for the decay chains reported here range from 700 to 30000 events.

4.1 Likelihood Function

The likelihood function incorporates a number of observables to distinguish signal from the large number of background events retained by the sample selection. We describe the B decay kinematics with two variables: ΔE and m_{ES} . We also include the mass of the primary resonance (m_η or $m_{\eta'}$) and a Fisher discriminant \mathcal{F} , which describes energy flow in the event. The Fisher discriminant combines four variables: the angles with respect to the beam axis of the B momentum and B thrust axis (in the $\Upsilon(4S)$ frame), and the zeroth and second angular moments $L_{0,2}$ of the energy flow about the B thrust axis. The moments are defined by $L_j = \sum_i p_i \times |\cos \theta_i|^j$, where θ_i is the angle with respect to the B thrust axis of track or neutral cluster i , p_i is its momentum, and the sum excludes the B candidate.

In addition to these four variables, we include the following observables relevant to particular decay chains. For modes with a K^* or ρ , we include in the fit the mass and helicity angle of the vector meson with a two-dimensional probability distribution function (PDF) accounting for the different shapes of the helicity-angle distributions for true K^* or ρ mesons in the background and for combinatoric background. To separate $\eta'\pi^+$ from $\eta'K^+$ we include in the PDF for the pion (kaon) signal the observable S_π (S_K), the Cherenkov angle residual with respect to the expected angle for pions (kaons) normalized by the measurement error.

As measured correlations among these observables in the selected data are small, we take the PDFs for each event i to be a product of the PDFs for the separate observables. We define hypotheses j , where j can be signal, continuum background, or (where appropriate) $B\bar{B}$ background. The PDF for the $\eta^{(\prime)}\rho$ and $\eta^{(\prime)}K^*$ analyses is given by

$$\mathcal{P}_j^i = \mathcal{P}_j(m_{\text{ES}}^i) \cdot \mathcal{P}_j(\Delta E^i) \cdot \mathcal{P}_j(\mathcal{F}^i) \cdot \mathcal{P}_j(m_{\eta^{(\prime)}}^i) \cdot \mathcal{P}_j(m_{K^*/\rho}^i, \mathcal{H}^i). \quad (1)$$

For the $\eta'\pi^+$ analysis, j separately indexes pion and kaon components:

$$\mathcal{P}_j^i = \mathcal{P}_j(m_{\text{ES}}^i) \cdot \mathcal{P}_j(\Delta E_j^i) \cdot \mathcal{P}_j(\mathcal{F}^i) \cdot \mathcal{P}_j(m_{\eta^{(\prime)}}^i) \cdot \mathcal{P}_j(S_j^i). \quad (2)$$

The likelihood function for each decay mode is

$$\mathcal{L} = \frac{\exp(-\sum_j Y_j)}{N!} \prod_i \sum_j Y_j \mathcal{P}_j^i, \quad (3)$$

where Y_j is the yield of events of hypothesis j to be found by the fitter, and N is the number of events in the sample. The first factor takes into account the Poisson fluctuations in the total number of events.

4.2 Signal and Background Parameterization

We determine the PDFs for signal from MC distributions in each observable. The PDFs for $B\bar{B}$ background (where appropriate) arise from fitting the composite $B\bar{B}$ MC sample, discussed in Section 3.2. For the continuum background we establish the functional forms and initial parameter values of the PDFs with data from sidebands in m_{ES} or ΔE . We then refine the main background parameters (excluding resonance mass central values and widths) by allowing them to float in the final fit.

The distributions in the resonance mass(es), m_{ES} , and ΔE for signal, are parameterized as Gaussian functions, with a second Gaussian as required for good fits to these samples. Slowly varying distributions (combinatoric background under the resonance mass and ΔE peaks) are parameterized by linear or quadratic functions. We find that two Gaussians also describe the ΔE shape in $B\bar{B}$ background, with one Gaussian typically peaking low (for feed-down) and the other centered high (for feed-up). The combinatoric background in m_{ES} is described by a phase-space-motivated empirical (ARGUS) function [20]. For $B\bar{B}$ background, we use an ARGUS function plus a Gaussian to parameterize m_{ES} . We model the \mathcal{F} distribution using a Gaussian function with different widths above and below the mean; in background, we include a second Gaussian or a linear contribution to account for outlying events. The additional terms ensure that the background is well modeled in the low-side tail region where signal is found.

The PDFs for the helicity angle variable \mathcal{H} are given by polynomials (quadratic in signal and continuum background, quartic in $B\bar{B}$ background). This function is multiplied by a Fermi-Dirac threshold function where needed to fit a drop in detector efficiency near $\mathcal{H} = +1$ or -1 where the energy of one of the resonance daughters is low. As there is a true resonance component in continuum background, we allow for different shapes in \mathcal{H} for those events corresponding to real K^* or ρ resonances as opposed to the combinatoric continuum.

The PDFs $\mathcal{P}(S_{\pi,K})$ are determined with a sample of D^* -tagged D^0 decays, and parameterized as double Gaussians. Consistent with the calibrations, the kaon PDFs for S and ΔE are copies of those for pions evaluated at the corresponding displaced value of the observable².

We check the simulation on which we rely for signal PDFs by comparing with large data control samples. For m_{ES} and ΔE we use the decays $B^- \rightarrow \pi^- D^0$ and $B^- \rightarrow \rho^- D^0$ with $D^0 \rightarrow K^- \pi^+ \pi^0$, which have similar topology to the modes under study. For the resonance masses we use inclusive resonance production in data. We adjust the means and widths of PDF parameterizations based on these control samples.

5 Fit Results

By generating (from PDF shapes) and fitting simulated samples of signal and background, we verify that our fitting procedure is functioning properly. We find that the minimum $-\ln \mathcal{L}$ value in the on-resonance sample lies well within the $-\ln \mathcal{L}$ distribution from these simulated samples.

The efficiency is obtained from the fraction of signal MC events passing the selection, adjusted for any bias in the likelihood fit. This bias is determined from fits to simulated samples, each equal in size to the data and containing a known number of signal (and $B\bar{B}$, where appropriate) MC events combined with events generated from the continuum background PDFs. The biases we find

²To facilitate simulations and PDF projections we actually work with the transformed pairs $(S_{\pi}, \delta S \equiv S_{\pi} - S_K)$ and $(\Delta E_{\pi}, \delta \Delta E \equiv \Delta E_K - \Delta E_{\pi})$

depend on the mode, but are a few percent where the yield is substantial, or at most 2–3 events in the limit of vanishing yield.

Table 3: Yields, efficiencies, branching fractions, and charge asymmetries for B decays to states with an η meson, measured with our sample of 89 million $B\bar{B}$ pairs. The overall yields and efficiencies (ϵ) of the combined mode are given as the sum of yields and efficiencies from the various daughter particle decay channels, and for these we incorporate the systematic errors.

Mode	Fit $\mathcal{B}(10^{-6})$	Signif. (σ)	Signal yield	ϵ (%)	\mathcal{A}_{ch}
$B^0 \rightarrow \eta K^{*0}$	$19.0^{+2.2}_{-2.1} \pm 1.3$	15	157	9.2	$+0.03 \pm 0.11 \pm 0.02$
$\eta_{\gamma\gamma} K^{*0}$	21 ± 3	13.1	125 ± 16	6.6	$+0.12 \pm 0.12$
$\eta_{3\pi} K^{*0}$	14 ± 4	6.8	32 ± 9	2.6	-0.39 ± 0.25
$B^+ \rightarrow \eta K^{*+}$	$25.7^{+3.8}_{-3.6} \pm 1.8$	12	113	4.7	$+0.15 \pm 0.14 \pm 0.02$
$\eta_{\gamma\gamma} K_{K^0_S \pi^+}^{*+}$	23 ± 6	5.7	46 ± 12	2.2	$+0.04 \pm 0.24$
$\eta_{3\pi} K_{K^0_S \pi^+}^{*+}$	32 ± 9	6.2	27 ± 8	0.9	$+0.46^{+0.24}_{-0.28}$
$\eta_{\gamma\gamma} K_{K^+\pi^0}^{*+}$	27 ± 8	6.0	30 ± 9	1.1	$-0.06^{+0.26}_{-0.27}$
$\eta_{3\pi} K_{K^+\pi^0}^{*+}$	20 ± 10	4.5	10 ± 5	0.5	$+0.39^{+0.41}_{-0.50}$
$B^+ \rightarrow \eta \rho^+$	$10.5^{+3.1}_{-2.8} \pm 1.3$	4.8	65	7.0	$+0.06 \pm 0.29 \pm 0.02$
$\eta_{\gamma\gamma} \rho^+$	10 ± 4	3.8	42 ± 17	4.7	$+0.46^{+0.34}_{-0.39}$
$\eta_{3\pi} \rho^+$	11 ± 6	3.0	23 ± 12	2.3	$-0.56^{+0.48}_{-0.24}$

In Tables 3 and 4 we show the results of the fits to the on-resonance data. Shown for each decay mode are the measured branching fraction and the 90% confidence level upper limit (where appropriate). We report the statistical significance for the individual decay chains and display the significance including systematics for the combined result in each channel. The statistical significance is taken as the square root of the difference between the value of $-2 \ln \mathcal{L}$ for zero signal and the value at its minimum. The tables also include the fit signal yield, where the statistical error on the number of events is taken as the change in the central value when the quantity $-2 \ln \mathcal{L}$ changes by one unit. The 90% C.L. upper limit is taken as the solution B to the condition $\int_0^B \mathcal{L}(b) db / \int_0^\infty \mathcal{L}(b) db = 0.9$. The overall efficiency is given by the product of the Monte Carlo efficiency, efficiency corrections, and branching fraction products for the daughter particle decay sequences. The number of produced B mesons is computed with the assumption of equal production rates of charged and neutral pairs. The final column in Table 3 gives the charge asymmetry (\mathcal{A}_{ch}).

In Figures 3 and 4, we show projections of m_{ES} and ΔE for the ηK^* and $\eta \rho^+$ modes, respectively. We make these plots by selecting events with signal likelihood (computed without the variable shown in the figure) exceeding a mode-dependent threshold that optimizes the expected sensitivity. The selection retains a fraction of the signal yield averaging about 70% across the decay sequences.

6 Systematic Uncertainties

Floating background parameters in the fit allows us to incorporate into the overall statistical error most of the systematic errors on yields that arise from uncertainties in the values of the PDF

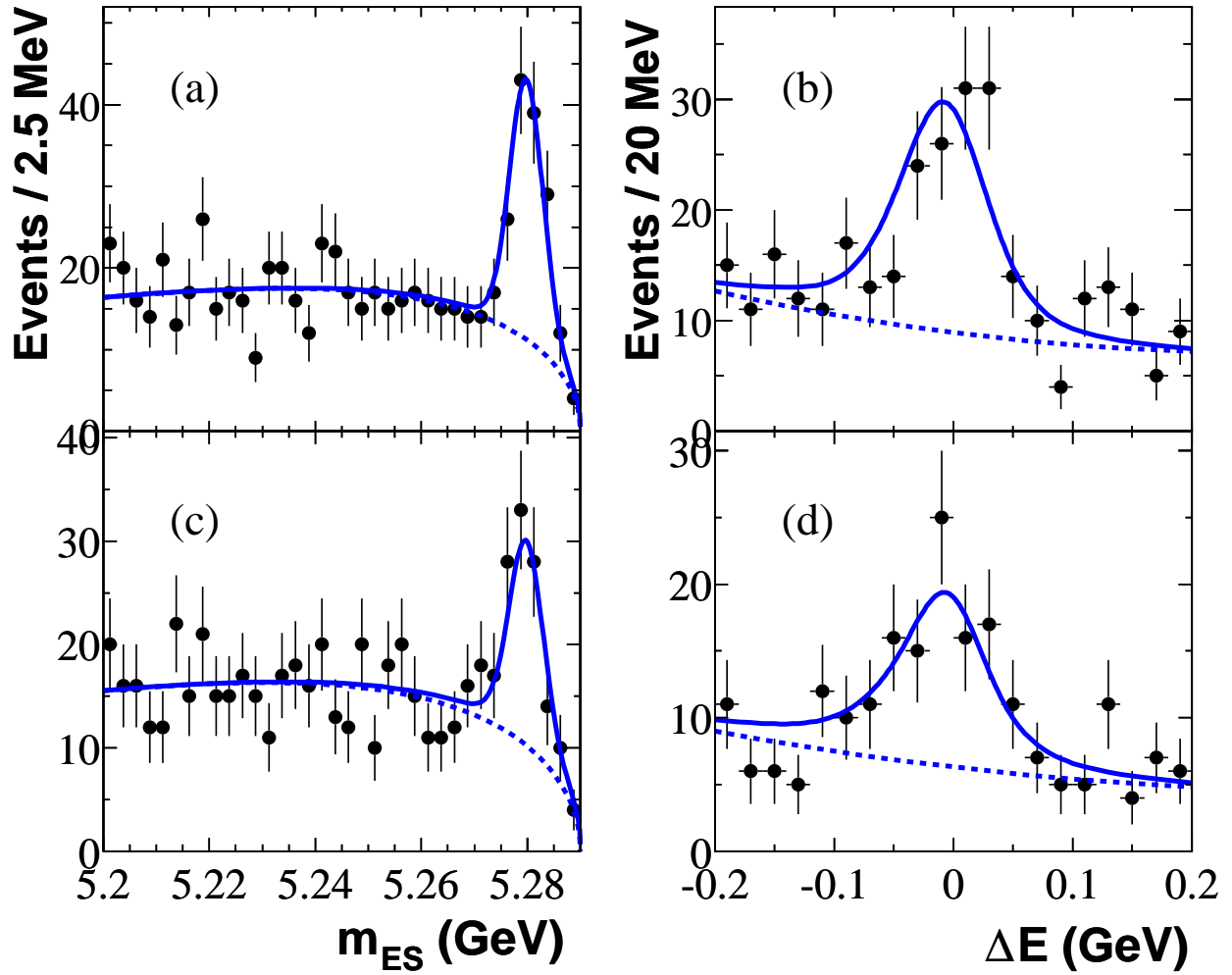


Figure 3: Projections of the B candidate m_{ES} and ΔE for ηK^{*0} (a, b) and ηK^{*+} (c, d). Points with errors represent data, solid curves the full fit functions, and dashed curves the background functions. These plots are made with a cut on the signal likelihood and thus do not show all events in the data samples.

Table 4: Yields, efficiencies, and branching fractions for B decays to states with an η' meson, measured with our sample of 89 million $B\bar{B}$ pairs. We quote 90% CL upper limits if the significance of the measured yield is less than 4 sigma. The overall yields and efficiencies (ϵ) of the combined mode are given as the sum of yields and efficiencies from the various daughter particle decay channels, and for these we incorporate the systematic errors.

Mode	Fit $\mathcal{B}(10^{-6})$	UL $\mathcal{B}(10^{-6})$	Signif. (σ)	Signal yield	ϵ (%)
$B^+ \rightarrow \eta' \pi^+$	$2.8^{+1.3}_{-1.0} \pm 0.3$	< 4.5	3.4	13	9.9
$\eta'_{\eta\pi\pi} \pi^+$	4 ± 2		3.9	17 ± 7	4.9
$\eta'_{\rho\gamma} \pi^+$	-1 ± 3		—	-4 ± 10	5.0
$B^0 \rightarrow \eta' K^{*0}$	$3.2^{+1.8}_{-1.6} \pm 0.9$	< 6.4	2.2	22	6.6
$\eta'_{\eta(\gamma\gamma)\pi\pi} K^{*0}$	-2 ± 2		—	-4 ± 4	2.3
$\eta'_{\eta(3\pi)\pi\pi} K^{*0}$	13 ± 6		2.8	11 ± 5	1.0
$\eta'_{\rho\gamma} K^{*0}$	5 ± 3		1.9	15 ± 10	3.4
$B^+ \rightarrow \eta' K^{*+}$	$6.1^{+3.9}_{-3.2} \pm 1.2$	< 12	2.4	15.4	3.0
$\eta'_{\eta\pi\pi} K_{K_S^0\pi^+}^{*+}$	-12 ± 5		—	-8 ± 4	0.8
$\eta'_{\rho\gamma} K_{K_S^0\pi^+}^{*+}$	16 ± 9		2.6	16 ± 9	1.1
$\eta'_{\eta\pi\pi} K_{K^+\pi^0}^{*+}$	7 ± 7		1.8	3 ± 3	0.5
$\eta'_{\rho\gamma} K_{K^+\pi^0}^{*+}$	8 ± 13		0.7	5 ± 7	0.6
$B^+ \rightarrow \eta' \rho^+$	$14.0^{+5.1}_{-4.6} \pm 1.9$	< 22	3.8	69	4.1
$\eta'_{\eta\pi\pi} \rho^+$	11 ± 6		3.1	17 ± 8	1.8
$\eta'_{\rho\gamma} \rho^+$	25 ± 12		2.8	52 ± 23	2.3

parameters. We determine the sensitivity to parameters of the signal PDF components by varying these within their uncertainties in all channels except for $\eta' \pi^+$. In the $\eta' \pi^+$ decay, we float the primary signal parameters and determine the effect on signal yield; this is possible because of the simultaneous fit with $\eta' K^+$, which has a large branching fraction. This is the only systematic error on the fit yield; the other systematics apply to either the efficiency or the number of $B\bar{B}$ events.

The uncertainty in our knowledge of the efficiency is found to be $0.8N_t\%$, $2.5N_\gamma\%$, and 3% for a K_S^0 decay, where N_t and N_γ are the number of signal tracks and photons, respectively. We estimate the uncertainty in the number of produced $B\bar{B}$ pairs to be 1.1%. The estimated error on systematic bias from the fitter itself (1–12%) comes from fits of simulated samples with varying signal and background populations. Published world averages [21] provide the B daughter branching fraction uncertainties. We account for systematic effects in $\cos\theta_T$ (1 – 3.5%, depending upon how tight a cut is made), in the PID requirements (2%), and from MC statistics (1.2%). For decay channels where a $B\bar{B}$ component is included in the fit, we assign an additional systematic determined by varying the $B\bar{B}$ yield within its errors. We quote the $B\bar{B}$ background systematic to be one half the measured change in the signal yield when the number of fit $B\bar{B}$ events is changed by one standard deviation. For the $\eta' \rho^+$ decay, where the fit $B\bar{B}$ background yield is about five times larger than other decays, we also vary the $B\bar{B}$ background model to account for different amounts of the expected individual backgrounds.

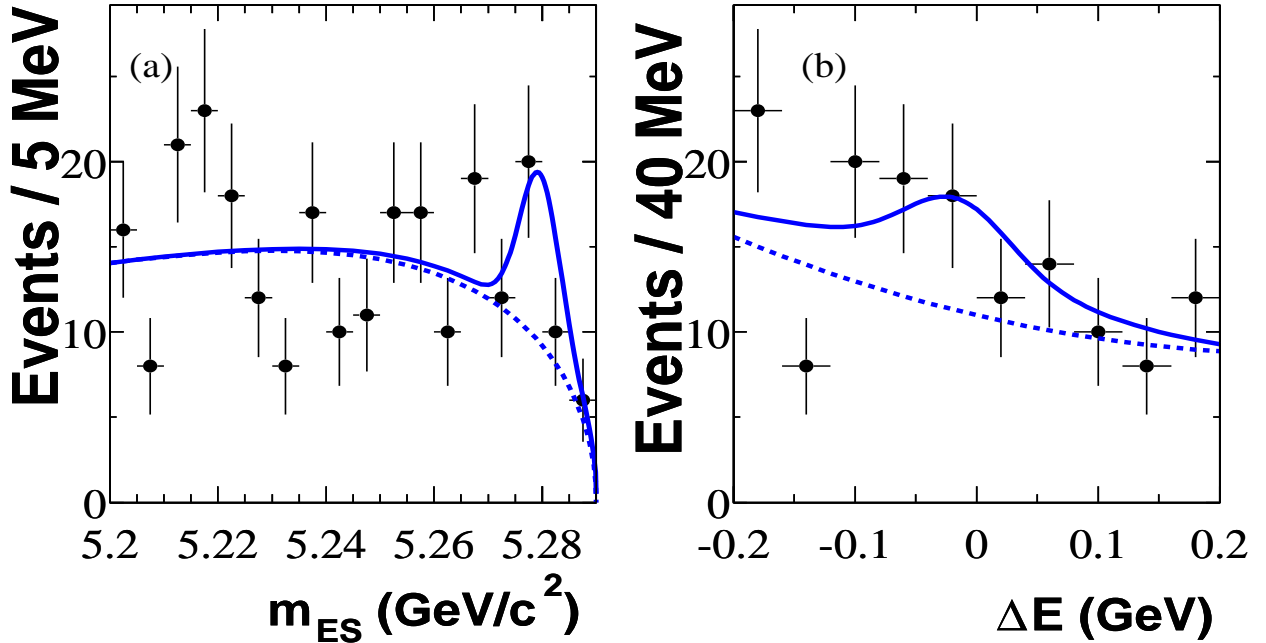


Figure 4: Projections of the B candidate m_{ES} (a) and ΔE (b) for $B^+ \rightarrow \eta\rho^+$. Points with errors represent data, solid curves the full fit functions, and dashed curves the background functions. These plots are made with a cut on the signal likelihood and thus do not show all events in the data samples.

A study of the charge asymmetry as a function of momentum for all tracks in hadronic events bounds the tracking efficiency component of charge-asymmetry bias to be less than 1%. D^* -tagged $D \rightarrow K\pi$ and B samples provide additional crosschecks that the bias is small. We assign a systematic uncertainty for \mathcal{A}_{ch} of 2% based on the tracking study and a small PID contribution determined from the D^* studies.

We keep track of which systematic error contributions are (un)correlated between the several measurements with different secondary decay modes of the same primary decay for use in obtaining their average as the final branching fraction result.

7 Combined Results

To obtain the final results we combine the branching fraction and charge asymmetry measurements from the individual daughter decay chains. The joint likelihood is given by the product, or equivalently $-2\ln\mathcal{L}$ is given by the sum, of contributions from the submodes. The statistical contribution comes directly from the likelihood fit, which reflects the non-Gaussian uncertainty associated with small statistics. Before combining we convolve each statistical $-2\ln\mathcal{L}$ with a Gaussian function representing the part of the systematic error that is uncorrelated among the submodes. We show the resulting distributions in Fig. 5 for our measurements of previously unseen decays that have significance greater than 3 sigma. The corresponding distributions without systematics give the combined statistical errors, and these in conjunction with the solid curves in Fig. 5 and the correlated systematics give the total systematic errors.

The resulting branching fractions and charge asymmetries are included in Tables 3 and 4, where

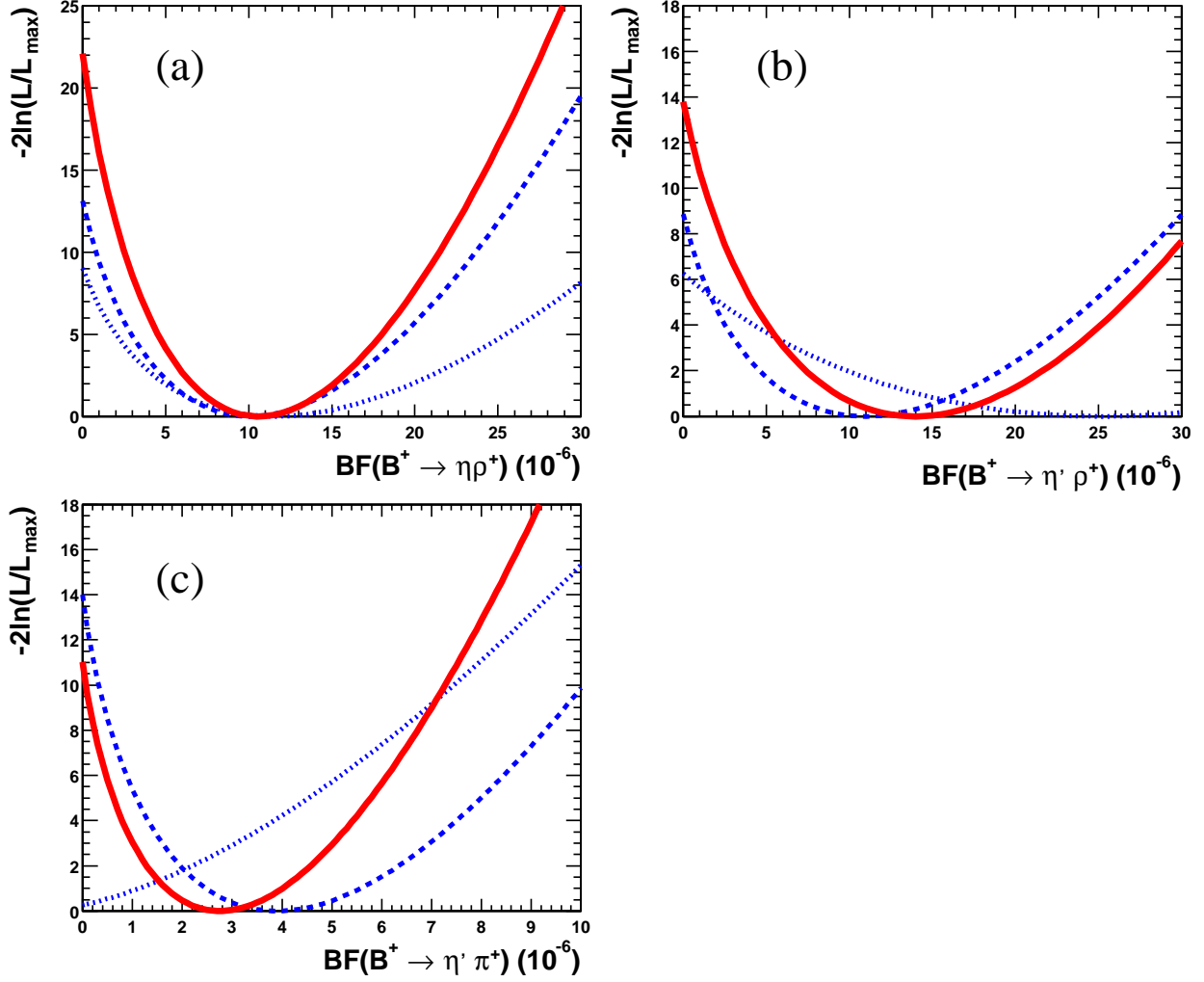


Figure 5: Distributions of $-2\ln\mathcal{L}$ convolved with uncorrelated systematic errors for branching fraction measurements. Solid curves represent the result of combining channels. The frames present (a) $\eta\rho^+$, with $\eta_{\gamma\gamma}\rho^+$ (dashed) and $\eta_{3\pi}\rho^+$ (dotted); (b) $\eta'\rho^+$, with $\eta'_{\eta\pi\pi}\rho^+$ (dashed) and $\eta'_{\rho\gamma}\rho^+$ (dotted); and (c) $\eta'\pi^+$, with $\eta'_{\eta\pi\pi}\pi^+$ (dashed) and $\eta'_{\rho\gamma}\pi^+$ (dotted).

the significance given includes systematics.

8 Conclusion

We report preliminary measurements of branching fractions and \mathcal{A}_{ch} for B meson decays to η or η' with a K^* , ρ^+ , or π^+ . We find signals with statistical significance exceeding four standard deviations in all η channels. The decay $B^+ \rightarrow \eta\rho^+$ has not been seen previously. We also have evidence for $B^+ \rightarrow \eta'\rho^+$ (with significance 3.8σ) and $B^+ \rightarrow \eta'\pi^+$ (with significance 3.4σ). The observed values in the η channels are

$$\begin{aligned}\mathcal{B}(B^0 \rightarrow \eta K^{*0}) &= (19.0_{-2.1}^{+2.2} \pm 1.3) \times 10^{-6}, \\ \mathcal{B}(B^+ \rightarrow \eta K^{*+}) &= (25.7_{-3.6}^{+3.8} \pm 1.8) \times 10^{-6}, \\ \mathcal{B}(B^+ \rightarrow \eta\rho^+) &= (10.5_{-2.8}^{+3.1} \pm 1.3) \times 10^{-6}.\end{aligned}$$

For the η' channels we find

$$\begin{aligned}\mathcal{B}(B^+ \rightarrow \eta'\pi^+) &= (2.8_{-1.0}^{+1.3} \pm 0.3) \times 10^{-6} (< 4.5 \times 10^{-6}), \\ \mathcal{B}(B^0 \rightarrow \eta'K^{*0}) &< 6.4 \times 10^{-6}, \\ \mathcal{B}(B^+ \rightarrow \eta'K^{*+}) &< 12 \times 10^{-6}, \\ \mathcal{B}(B^+ \rightarrow \eta'\rho^+) &= (14.0_{-4.6}^{+5.1} \pm 1.9) \times 10^{-6} (< 22 \times 10^{-6}),\end{aligned}$$

where the upper limits are taken at 90% CL. These results supersede the previous *BABAR* measurements [14, 15]. They represent substantial improvements over all previous measurements, as can be seen from Tables 1 and 2. The branching fraction limit for $B^+ \rightarrow \eta'\pi^+$ is nearly three times more restrictive than previous measurements. The measurement for $B \rightarrow \eta'K^*$ is not yet precise enough to determine whether a flavor singlet component is present for this decay, though we do restrict the size of this contribution.

For the modes with significant signals, we measure the charge asymmetries

$$\begin{aligned}\mathcal{A}_{ch}(\eta K^{*0}) &= +0.03 \pm 0.11 \pm 0.02, \\ \mathcal{A}_{ch}(\eta K^{*+}) &= +0.15 \pm 0.14 \pm 0.02, \\ \mathcal{A}_{ch}(\eta\rho^+) &= +0.06 \pm 0.29 \pm 0.02.\end{aligned}$$

These charge asymmetry results are in agreement with the theoretical expectations discussed in Section 1 and rule out substantial portions of the physical region.

9 Acknowledgments

We are grateful for the extraordinary contributions of our PEP-II colleagues in achieving the excellent luminosity and machine conditions that have made this work possible. The success of this project also relies critically on the expertise and dedication of the computing organizations that support *BABAR*. The collaborating institutions wish to thank SLAC for its support and the kind hospitality extended to them. This work is supported by the US Department of Energy and National Science Foundation, the Natural Sciences and Engineering Research Council (Canada), Institute of High Energy Physics (China), the Commissariat à l'Énergie Atomique and Institut National de Physique Nucléaire et de Physique des Particules (France), the Bundesministerium für

Bildung und Forschung and Deutsche Forschungsgemeinschaft (Germany), the Istituto Nazionale di Fisica Nucleare (Italy), the Foundation for Fundamental Research on Matter (The Netherlands), the Research Council of Norway, the Ministry of Science and Technology of the Russian Federation, and the Particle Physics and Astronomy Research Council (United Kingdom). Individuals have received support from the A. P. Sloan Foundation, the Research Corporation, and the Alexander von Humboldt Foundation.

References

- [1] CLEO Collaboration, B. H. Behrens *et al.*, Phys. Rev. Lett. **80**, 3710 (1998).
- [2] H. J. Lipkin, Phys. Lett. B **254**, 247 (1991).
- [3] C.-W. Chiang and J. L. Rosner, Phys. Rev. D **65**, 074035 (2002).
- [4] M. Beneke and M. Neubert, Nucl. Phys. B **651**, 225 (2003).
- [5] BABAR Collaboration, B. Aubert *et al.*, BABAR-PUB 03/006, hep-ex 0303046 (2003).
- [6] BABAR Collaboration, B. Aubert *et al.*, BABAR-CONF 03/009, hep-ex 0303039 (2003).
- [7] G. Kramer, W.F. Palmer, and H. Simma, Nucl. Phys. B **428**, 77 (1994).
- [8] A. Ali, G. Kramer, and C. D. Lü, Phys. Rev. D **58**, 094009 (1998); Y. H. Chen *et al.*, Phys. Rev. D **60**, 094014 (1999); H.-Y. Cheng and K.-C. Yang, Phys. Rev. D **62**, 054029 (2000); N.G. Deshpande, B. Dutta, and Sechul Oh, Phys. Lett. B **473**, 141 (2000); M. Gronau, and J.L. Rosner, Phys. Rev. D **61**, 073008 (2000); H.K Fu, X.G. He, Y.K. Hsaio, hep-ph/0304242.
- [9] M.-Z. Yang and Y.-D. Yang, Nucl. Phys. B **609**, 469 (2001).
- [10] C.-W. Chiang, M. Gronau, and J.L. Rosner, hep-ph/0306021.
- [11] A. Ali, G. Kramer, and C.-D. Lü, Phys. Rev. D **59**, 014005 (1999). These authors use the opposite sign convention for \mathcal{A}_{ch} than the one used in this paper.
- [12] A.S. Dighe, M. Gronau, and J.L. Rosner, Phys. Rev. Lett. **79**, 4333 (1997).
- [13] CLEO Collaboration, S. J. Richichi *et al.*, Phys. Rev. Lett. **85**, 520 (2000).
- [14] BABAR Collaboration, B. Aubert *et al.*, Phys. Rev. Lett. **87**, 221802 (2001).
- [15] P. Bloom, Proceedings of the 2002 SLAC Summer Institute, hep-ex/0302030 (2003).
- [16] H.C. Huang (for the Belle Collaboration), hep-ex/0205062 (Moriond 2002 Contributed paper) (2002); Belle Collaboration (K. Abe *et al.*), BELLE-CONF-0137 (Lepton-Photon 2001 Contributed paper), 2001.
- [17] BABAR Collaboration, B. Aubert *et al.*, Nucl. Instr. Meth. A **479**, 1 (2002).
- [18] PEP-II Conceptual Design Report, SLAC-R-418 (1993).
- [19] The BABAR detector Monte Carlo simulation is based on GEANT4, S. Agostinelli *et al.*, Nucl. Instr. Meth. A **506**, 250 (2003).

- [20] With $x \equiv m_{ES}/E_b$ and ξ a parameter to be fit, $f(x) \propto x\sqrt{1-x^2} \exp[-\xi(1-x^2)]$. See ARGUS Collaboration, H. Albrecht *et al.*, Phys. Lett. B **241**, 278 (1990).
- [21] Particle Data Group, K. Hagiwara *et al.*, Phys. Rev. D **66**, 010001 (2002).